



UNIVERSITY OF LEEDS

This is a repository copy of *Characterisation of temporal variations of alkali-activated slag cement property using microstructure features and electrical responses*.

White Rose Research Online URL for this paper:  
<https://eprints.whiterose.ac.uk/163463/>

Version: Accepted Version

---

**Article:**

Zhu, X, Li, Q, Yang, K et al. (5 more authors) (2020) Characterisation of temporal variations of alkali-activated slag cement property using microstructure features and electrical responses. *Construction and Building Materials*, 261. 119884. ISSN 0950-0618

<https://doi.org/10.1016/j.conbuildmat.2020.119884>

---

© 2020, Elsevier Ltd. This manuscript version is made available under the CC-BY-NC-ND 4.0 license <http://creativecommons.org/licenses/by-nc-nd/4.0/>.

**Reuse**

This article is distributed under the terms of the Creative Commons Attribution-NonCommercial-NoDerivs (CC BY-NC-ND) licence. This licence only allows you to download this work and share it with others as long as you credit the authors, but you can't change the article in any way or use it commercially. More information and the full terms of the licence here: <https://creativecommons.org/licenses/>

**Takedown**

If you consider content in White Rose Research Online to be in breach of UK law, please notify us by emailing [eprints@whiterose.ac.uk](mailto:eprints@whiterose.ac.uk) including the URL of the record and the reason for the withdrawal request.



[eprints@whiterose.ac.uk](mailto:eprints@whiterose.ac.uk)  
<https://eprints.whiterose.ac.uk/>

1     **Characterisation of temporal variations of alkali-activated slag cement property**  
2                     **using microstructure features and electrical responses**

3     Xiaohong Zhu<sup>1,2</sup>, **Qing Li<sup>1\*</sup>**, **Kai Yang<sup>1,2\*</sup>**, Song Mu<sup>3</sup>, Zhilu Zhang<sup>1</sup>, Bryan Magee<sup>4</sup>, Changhui Yang<sup>1</sup>,  
4     Muhammed Basheer<sup>2</sup>

5     1) College of Materials Science and Engineering, Chongqing University, Chongqing, China

6     2) School of Civil Engineering, University of Leeds, Leeds, UK

7     3) Jiangsu Provincial Institute of Building Science, Nanjing, China

8     4) Built Environment Research Institute, Ulster University, Ulster, UK

9     **Abstract**

10    Relatively few studies currently exist concerning temporal variation of the overall performance of  
11    alkali-activated slag (AAS) cement; a topic essential for quality control in practice. This study uses  
12    microstructural characteristics and electrical responses to reflect performance variation of AAS cement.  
13    To achieve this, four key performance parameters were assessed, pore formation factor, chloride  
14    transport coefficient, permeability coefficient and compressive strength. Classical theories used for  
15    PC-based materials were applied to estimate the performance of AAS paste. It is found that the  
16    formation factor of AAS can be assessed by combining bulk conductivity and pore solution  
17    conductivity and the permeation properties of AAS cement cannot be reliably assessed by the Katz-  
18    Thomson (KT) model, while the Millington-Quirk (MQ) model works better. To assess the  
19    relationship between compressive strength and permeable porosity, the Balshin and Ryshkevitch  
20    equations performed best in terms of describing the relationship between these two parameters.  
21    Meanwhile, AAS cement is more sensitive to the mix proportions and additional care is needed to  
22    ensure its quality. It is the first time to use electrical response to predict the chloride transport  
23    coefficients of AAS cement, which would provide a powerful tool for its quality control and service  
24    life prediction.

25    **Keywords:** alkali-activated slag cement, microstructure features, electrical responses, pore formation  
26    factor, permeation properties, strength development

27

## 1. Introduction

Owing to remarkable economic growth and high speeds of construction in the last 40 years, China has become the world's largest cement producer, responsible for nearly 60% of Portland cement (PC) manufactured worldwide [1]. With cement production closely related to key environmental concerns such as energy consumption and CO<sub>2</sub> emission, several viable alternatives that provide supplementary choice and/or improvement to conventional PC systems are the focus of a vibrant research area.

Use of industry-by-products is an established way to reduce uses of PC clinker [2-4]. Reflecting the size of China's steel industry [5, 6], ground granulated blast-furnace slag (GGBS) has emerged as a main supplementary cementitious material (SCM) used both as a partial replacement for PC to improve the performance of conventional concrete, and also to manufacture alkali-activated slag (AAS) cement-based materials [7, 8].

AAS cement was formally invented in 1957 by Glukhovsky at the Kiev Institute of Civil Engineering, Ukraine, although the possibility of using alkaline activation of slag can be traced back earlier [9-11]. Previous research [12-15] has shown that AAS binding systems have several advantages over PC, such as rapid and high compressive strength, low heat of hydration, high temperature and corrosion resistance against chemical attacks and/or from high chloride concentration situations. While practical AAS applications are being reported worldwide [16-18], its widespread adoption requires in-depth understanding of its disadvantageous properties, including controlled setting behaviour, occurrence of efflorescence [19], shrinkage and micro-cracking [20-23], and suitable water reducing techniques [9]. In addition, urgently needed are established techniques to control and predict long-term AAS properties.

It is known [2,17,19] that standard core analysis is not always able to predict the overall performance of AAS-based materials, with high statistical variance of results failing to provide sufficient information concerning all processes which may be occurring. Microstructural features and electrical responses can be used to assess and predict transport and mechanical properties of PC and relevant techniques can provide satisfactory results [24]. Despite this, special care is still needed when using these approaches to assess AAS performance [17], due to the significant differences in physical and chemical characteristics that exist between the two binder systems.

Therefore, four key performance parameters, including formation factor, permeability, diffusivity and compressive strength, were used to characterise the performance of AAS cement pastes. To achieve this, compressive strength, bulk conductivity, pore solution conductivity, accessible porosity and pore size distribution were all measured. Further comparisons were made to examine if established techniques for PC-based systems were applied to AAS cement-based materials.

## 2. Theoretical consideration

### 2.1 Estimation of pore formation factor

An essential parameter describing transport properties, pore formation factor is the ratio of fluid path length to the length of the sample, which is a function of porosity and pore connectivity. Determination of formation factor is not straightforward as the micro-geometry of cementitious materials are characterised by mesoscale heterogeneities. As such, fluid molecules are unable to sample the representative volume of pore space in the experimentally accessible measurement time. It has been observed [24] that when measuring the flow of electric current through fully saturated samples, path connectivity is dependent on the conducting fluid and the microstructure characteristics, while electrical resistivity is a simple function of porosity and average length of path. As the flow of fluid and electric current in many aspects are analogous, electrical measurements in cementitious materials can be described using:

$$\rho_T = \rho_o \cdot \frac{1}{\beta \cdot \phi} \quad \text{Eq 1}$$

where:  $\rho_T$  is the total resistivity ( $\Omega$ );  $\rho_o$  is the resistivity of the pore solution, which is a function of ion composition and concentration in solution ( $\Omega$ );  $\phi$  is the porosity of the system accessible to fluids; and  $\beta$  is the connectivity of the pores in the system, which characterises how capillary pores are connected in a three-dimensional system. The resistivity of a saturated sample solely depends on the two microstructural parameters (porosity  $\phi$ , and connectivity  $\beta$ ). As it is often difficult to differentiate between these two terms, the literature [24] presents their product, which inversely is referred to as the formation factor,  $F$ , where:

$$\beta \cdot \phi = \frac{1}{F} \quad \text{Eq 2}$$

Formation factor is a material property that is independent of specimen size or shape, but relies on the characteristics of the medium. Further, the formation factor is also referred to as a transport property, as it can be used to analyse the diffusivity of porous materials. As such, an accurate estimate of formation factor is of particular significance.

### 2.2 Estimation of ion diffusion coefficient

Diffusion is the process by which ions move through pore solution due to differences in concentration, and is often considered as the main transport mechanism for chloride ions in saturated cementitious materials. According to Brownian motion, the mean-square displacement of molecules is linearly proportional to time in bulk fluids. The proportionality constant is the bulk diffusion coefficient,  $D_o$ . The formation factor is related to the diffusion coefficient by the established Nernst-Einstein equation, as follows:

$$1 \quad \frac{\rho_T}{\rho_o} = F = \frac{D_o}{D} \quad \text{Eq 3}$$

2 where:  $D_o$  is the self-diffusion coefficient describing how different ionic species move through  
 3 dilute solutions ( $\text{m}^2/\text{s}$ ); and  $D$  is the bulk diffusion coefficient ( $\text{m}^2/\text{s}$ ). The self-diffusion coefficient,  
 4  $D_o$ , can be determined for different ionic species. For chloride ions at 25 °C, a typical value in pure  
 5 water is  $2.03 \times 10^{-9} \text{ m}^2/\text{s}$  [25, 26].

6 Through the formation factor, the diffusion coefficient is closely connected to many transport  
 7 properties of fluids confined in AAS cement samples, including permeability, electrical conductivity  
 8 of electrolytes, and velocity of sound.

### 9 *2.3 Estimation of permeability coefficient*

10 Permeability is a key material property of durability assessment related to pore geometry rather than  
 11 the material's pore fluid. Modelling this parameter is a long-standing challenge as the permeability of  
 12 cementitious materials can vary by over five orders of magnitude. Even for concretes with the same  
 13 mixture proportions, variation of permeability can span three orders of magnitude [4, 27, 28]. Several  
 14 methods can be used to estimate permeability using microstructure properties. The first, derived from  
 15 Carman, is based on tortuosity and shape factor [29-31]. As this model contains pore radius and fluid  
 16 path length and some not directly measurable properties, it has not been considered in this study. The  
 17 second equation to describe saturated porous systems is the Katz-Thomson model [32-34], which  
 18 introduces the term critical pore diameter,  $d_c$  (m), to assess permeability,  $K_{KT}(\text{m}^2)$ , through formation  
 19 factor ( $F$ ) and the critical pore diameter as follows:

$$20 \quad K_{KT} = \frac{1}{226 \cdot F} \cdot d_c^2 \quad \text{Eq 4}$$

21 The third method uses the concept of series parallel arrangements of pores arising from random  
 22 apposition of planes within cementitious materials. Millington and Quirk [35] describe the  
 23 permeability,  $K_{MQ}(\text{m}^2)$ , of rock using the formation factor ( $F$ ) and the average pore radius:

$$24 \quad K_{MQ} = \frac{\overline{r^2}}{8F} \quad \text{Eq 5}$$

25 As shown in **Eq (4)** and **(5)**, both critical pore diameter and average pore radius are used to  
 26 estimate permeability coefficients. It has been noted that X-ray computed micro-tomography ( $\mu\text{CT}$ )  
 27 offers three-dimensional imaging of the pore structure in building materials, while at present most  
 28 instruments are unable to resolve components of porosity smaller than 5  $\mu\text{m}$  routinely [36, 37].  
 29 Moreover, direct measurement by quantitative image analysis in principle is a good way to estimate  
 30 the internal distribution of pores, but in practice, agreement between porosity estimated by image  
 31 analysis and other methods is often poor [37, 38]. One general reason for this is that it is difficult to  
 32 detect pores of widely different sizes in images of fixed magnification. In other words, the method has

1 limited dynamic range. As such, mercury intrusion porosimetry (MIP) was used to obtain these two  
2 parameters. While MIP has received criticism for its accuracy [39, 40], it can provide useful  
3 information about threshold diameter; a parameter representative of cement permeability [34, 41]. As  
4 such,  $\bar{r}$ , pore structure of AAS cement was characterised in this study by MIP.

#### 5 **2.4 Estimation of strength development from microstructure characteristics**

6 Compressive strength is the most sought-after property during the fabrication of concrete and  
7 numerous works have been carried out to analyse different influencing parameters [42-45]. It is  
8 generally recognised that the presence of pores affects strength adversely, despite different geometries  
9 of pores having different influences. Researchers [43,44] have attempted to establish links between  
10 porosity and compressive strength of cementitious materials, and the effectiveness of the following  
11 four equations is examined in this study.

12 Balshin's equation:  $\sigma = \sigma_0 \cdot (1 - \phi)^a$  Eq 6-1

13 Ryshkevitch's equation:  $\sigma = \sigma_0 \cdot e^{-b\phi}$  Eq 6-2

14 Schiller's equation:  $\sigma = c \cdot \ln\left(\frac{\phi_{CR}}{\phi}\right)$  Eq 6-3

15 Hasselman's equation:  $\sigma = \sigma_0 \cdot (1 - A\phi)$  Eq 6-4

16 Where:  $\sigma_0$  is the compressive strength at zero porosity (MPa);  $\sigma$  is the compressive strength  
17 at porosity  $\phi$  (MPa);  $\phi$  is the porosity (% by volume);  $\phi_{CR}$  is the porosity at zero strength (% by  
18 volume); a, b, c, k are empirical constants. Although  $\sigma_0$  can be interpreted as compressive strength  
19 at zero porosity, its value may not provide reliable response as strength can be affected by many other  
20 microscopic flaws not considered explicitly in these four models.

21

### 22 **3. Experiment programme**

#### 23 **3.1 Raw materials**

24 The raw material used to prepare the AAS samples in this study was GGBS from Chongqing Iron and  
25 Steel Group. Its specific gravity and Blaine fineness were 2.80 g/cm<sup>3</sup> and 430 m<sup>2</sup>/kg respectively.  
26 Conventional PC manufactured from Chongqing Fuhuang Cement Plant was used for the reference  
27 samples. The chemical composition of the GGBS and PC used are given in **Table 1**.

1 The activating alkaline was a commercial sodium silicate solution with a modulus (SiO<sub>2</sub>/Na<sub>2</sub>O  
2 molar ratio) of 2.46, a chemical composition of 29.03 wt.% SiO<sub>2</sub>, 12.07wt.% Na<sub>2</sub>O and 51.40% H<sub>2</sub>O.  
3 Chemically pure NaOH was used to adjust the modulus of sodium silicate to 1.2. The binders were  
4 prepared at activator (Na<sub>2</sub>O) concentrations of 5 wt.% of GGBS. Alkaline solutions were prepared and  
5 allowed to cool to room temperature prior to mixture preparation.

### 6 **3.2 Sample manufacture and curing regime**

7 Paste samples with W/B ratios of 0.35 and 0.50 were prepared for both the AAS and PC samples.  
8 Selection of these two W/B ratios is mainly based on previous experiences [14,17], as these parameters  
9 could cover the compressive strength from C30 to C60. Binder powder was added to the liquid and  
10 mixed for 3 mins in a planetary-type mixer. Pastes were cast into 40 mm cubes and  $\Phi 40 \times 100$  mm  
11 cylinders (for exacting pore solution) and immediately covered with plastic sheeting to minimise  
12 superficial drying. All samples were demoulded after 1 day and placed in a water bath at constant  
13 temperature (20  $\pm$  2 °C). Three samples were withdrawn for subsequent testing at 1, 3, 7, 14 and 28  
14 days.

### 15 **3.3 Test methods**

#### 16 **3.3.1 Accessible porosity**

17 Accessible porosity was examined via measurement of capillary porosity. It was determined on mass  
18 differences between water-saturated and dried pastes at different temperatures according to previous  
19 studies [46, 47]. After 3, 7, 14 and 28 days, samples were crushed to particle sizes around 10 mm and  
20 immersed in a solution of absolute ethyl alcohol to stop hydration. Samples were dried in a 40 °C  
21 vacuum oven until constant mass was achieved, which was recorded as  $M_{40^\circ C}$  (g). Dried samples were  
22 then immersed in deionised water for 24 hours, after which the saturated surface dry mass was recorded  
23 as  $M_s$  (g). The volume of crushed samples was determined using Le Chatelier Flask's method [48] and  
24 the capillary porosity computed using the following equation:

$$25 \quad \phi = \frac{M_s - M_{40^\circ C}}{\rho_w \cdot V} \times 100\% \quad \text{Eq 7}$$

26 where:  $\phi$  is the capillary porosity (% by volume);  $M_s$  is the mass of saturated sample (g);  $M_{40^\circ C}$   
27 is the constant mass of samples dried at 40 °C (g);  $\rho_w$  is the density of water (g/cm<sup>3</sup>); and  $V$  is the bulk  
28 volume of cement paste (cm<sup>3</sup>).

#### 29 **3.3.2 Bulk electrical conductivity**

30 Resistivity of paste samples was tested with a two-point uniaxial method via an LCR bridge. Prior to  
31 measurements, excess surface moisture was removed and specimens were placed between two thin  
32 parallel metal plates with moist sponges added to ensure effective electrode connection. Alternating  
33 (AC) voltage with a frequency of 1 kHz was applied in order to reduce effects of polarisation [49, 50].

1 The conductivity (S/m) of each specimen was calculated as the inverse of electrical resistivity, which  
2 was assessed using the following equation:

$$3 \quad \rho = R \frac{A}{l} \quad \text{Eq 8}$$

4 where:  $\rho$  is the electrical resistivity ( $\Omega \cdot \text{m}$ );  $R$  is the resistance of a uniform specimen ( $\Omega$ );  $A$  is  
5 the cross-section area of a specimen ( $\text{m}^2$ ); and  $l$  is the length of the specimen (m).

### 6 **3.3.3 Conductivity of ion liquid**

7 Pore fluids were extracted using the steel die press method following the protocol outlined by  
8 Vollpracht *et al* [51] and Barneyback and Diamond [52]. On the day before each test, specimens were  
9 removed from the aforementioned water tank and pre-conditioned in a standard environment ( $20 \pm 1$  °C,  
10  $\text{RH} \geq 95\%$ ) for 24 hours to achieve a saturated surface-dry state. Samples were loaded into the  
11 apparatus and the equipment was used in conjunction with a compression machine as shown **Figure**  
12 **1**. Pore solution was extracted under a constant pressure of 407.6 MPa (800 kN over  $1962.5 \text{ mm}^2$ ); a  
13 process taking around 45 minutes. The pore fluid was collected in 10-ml plastic syringes and then  
14 transferred to 50ml plastic bottles to minimise the potential carbonation effects until next analysis.  
15 Electrical conductivity of the pore solution was tested by a conductivity probe (Company: INESA,  
16 DDS-11a).

### 17 **3.3.4 Mercury intrusion porosimetry**

18 The pore size distribution of AAS and PC paste samples was determined using MIP. After curing for  
19 3, 7, 14 and 28 days, a sample was crushed to obtain the particle size of around 2 mm. Before MIP  
20 measurements, these samples were immersed in ethyl alcohol for 1 day and were moderately dried in  
21 a vacuum oven at 40 °C until constant weight was achieved. The porosimeter (MicromeriticsI, mode:  
22 Autopore 9500) was capable of minimum and maximum intruding pressures of 0.53 psi (26.90 mmHg)  
23 and 60000 psi (413.69 MPa) respectively. All these operations were automated by microcontroller and  
24 conducted within a fully enclosed pressure chamber. Incremental pore volume of each measured pore  
25 diameter,  $d$ , was calculated by assuming cylindrical pore and Washburn equation **Eq (9)**,

$$26 \quad d = -4 \cdot \frac{\gamma \cos\theta}{P} \quad \text{Eq 9}$$

27 where:  $\gamma$  is the surface tension of mercury, 0.485 N/m at 25 °C;  $P$  is the intrusion pressure  
28 ( $\text{N}/\text{m}^2$ );  $\theta$  is the wetting angle for mercury, assuming to be  $130^\circ$ . The threshold pore size,  
29 corresponding to the peak in the pore size-differential volume relationship, is found to be effective in  
30 the comparative studies [34, 53] and it has been used for permeability predictions [32-34, 54].

### 31 **3.3.5 Compressive strength**

1 Compressive strengths were determined in accordance with the National Standard GB/T 17671-1999  
2 [55] at ages of 3, 7, 14 and 28 days. All the results of compressive strength reported are the average  
3 value of three specimens.

## 4 **4. Results and discussion**

### 5 *4.1 Temporal property changes*

#### 6 **4.1.1 Compressive strength and porosity**

7 **Figure 2** summarises the compressive strength results obtained for the AAS and PC paste samples,  
8 and clearly indicates that decreasing W/B ratio and increasing age led to an increase in compressive  
9 strength for both binders. For all samples, rapid increase of compressive strength occurred for the first  
10 14 days, after which values stabilised. While AAS samples with a W/B ratio of 0.35 exhibited the most  
11 rapid rate of early age strength gain and the highest recorded values among the four sample types  
12 considered, an opposite trend was observed for the 0.50 W/B ratio AAS samples. More specifically,  
13 compressive strengths recorded for the 0.50 W/B ratio AAS before 7 days were significantly lower  
14 than for the corresponding PC samples. This observation contradicts commonly reported conclusions  
15 that AAS has fast hydration reaction rates and homogeneous hydration products [14, 56, 57].

16 The strength development values and mechanical behaviour of AAS may generally be attributed  
17 to the degree of porosity, hydration rate and distribution of hydration products. It is known that early-  
18 age reaction of AAS cement is based on alkali-mediated dissolution and precipitation. Monitored by  
19 backscattered electron mode scanning electron microscope, microstructural evolution occurs as rapid  
20 product formation occurs on the surface of GGBS grains in sodium silicate-activated systems, followed  
21 by a slow formation processes occurring internally. In this process, nucleation of AAS from the  
22 solution is dominated by the speed of precipitation of a gel like CSH phase, which fills the former pore  
23 space. This is different in nature from the needle-like outer product CSH in PC systems and, in contrast,  
24 forms bridging among the clinker grains [14, 58-60]. During the hydration of AAS, the molarity,  
25 concentration and type of alkali activators are key influential parameters. When the W/B ratio is low,  
26 silicate ion dissociation gains a higher alkalinity along with the liberation of  $\text{Ca}^{2+}$ , and in turn results  
27 in fast precipitation of CSH hydration at early stages [61, 62]. This phenomenon accounts for the more  
28 rapid strength gains noted for the AAS samples relative to the PC. Increase of W/B ratio from 0.35 to  
29 0.50 yielded a lower concentration of alkaline for a given alkaline content and it appears that the  
30 dissolution of GGBS needed more time and a lower alkali concentration to occur naturally. This means  
31 that a longer duration is needed for AAS hydration product and skeleton formation, as products and  
32 the rate of formation around slag grains rely on the availability of ions in the pore solution [63-65].  
33 The work certainly suggests that the effect of W/B ratio is more notable for AAS paste in comparison  
34 to PC.

1           **Figure 3** shows the variation of porosity for the AAS and PC paste samples with time. It can be  
2 seen that the porosity for all samples decreases significantly as age increases, especially before 7 days.  
3 Relative to all other samples, the porosity of W/B ratio 0.50 AAS samples remained high until 3 days,  
4 dropped by 30% between 3 and 14 days, and stabilised thereafter at a value of around 42%. In  
5 comparison, all other samples behaved similarly after 28 days, with porosities around 30%.  
6 Unsurprisingly, porosity was affected by extra water in the matrix, as higher W/B ratios tend to produce  
7 weaker matrices with higher capillary porosities; a trend particularly apparent for AAS mixes [66, 67].  
8 For the AAS-0.50 samples, porosity reduced rapidly after 3 days suggesting that in contrast to the slow  
9 dissolution process, precipitation of hydration products in AAS is relatively fast after saturation is  
10 reached. The reason for higher porosity in the AAS-0.50 mixes is that there is a substantially lower  
11 amount of gel formed. Similarly, Al-Otaibi [68] reported that decreasing Na<sub>2</sub>O dosages in AAS  
12 concrete resulted in an increase in porosity. When considering compressive strength and porosity  
13 results in combination, while the AAS-0.35 and PC-0.35 mixes had similar porosities after 28 days,  
14 the AAS pastes achieved higher strength, indicating stronger hydration products for the AAS systems.

15           **Figure 2** and **3** highlight the fact that the kinetics of chemical reaction between GGBS and  
16 activator is a complicated process, and that the influence of W/B ratio on strength development and  
17 porosity is more notable for AAS. High variability of AAS properties has been widely reported by  
18 different researchers [9, 14, 56, 63, 64, 69, 70], with influencing factors including the source,  
19 composition and fineness of the GGBS used, the type and dosage of the alkali activator, W/B ratio and  
20 the curing regime used. The results obtained in this study suggest that in order to control the quality of  
21 AAS, a deep and comprehensive consideration of raw materials, mix proportions and manufacturing  
22 process must be given.

#### 23 **4.1.2 Electrical responses**

24 Electrical conductivity of bulk samples and pore solutions at different ages for both AAS and PC  
25 samples are shown in **Figure 4**. As seen in **Figure 4 (a)**, the bulk electrical conductivity for AAS and  
26 PC progressively decreased as age increased. Bulk conductivity of samples saturated with conducting  
27 fluid is controlled by the saturating medium and pore structure parameters including overall porosity  
28 and pore geometry [64, 71, 72]. Ongoing hydration reactions make pores finer and less continuous,  
29 thereby naturally lowering bulk electrical conductivity.

30           Two distinguishable features can be seen in **Figure 4 (a)**. The first is that AAS samples had  
31 significantly higher conductivity than PC samples at equivalent ages, particularly before 7 days and  
32 that AAS sample porosity continuously decreased with curing process until 28 days; at which point  
33 similar values to the PC samples were achieved. This trend was particularly true for the AAS-0.50  
34 samples, which exhibited the highest bulk conductivity before 14 days and then similar values as the  
35 PC samples at 28 days. Justification for this is a combination of pore structure changes and higher pore  
36 solution conductivity contributed by the high Na<sup>+</sup> and OH<sup>-</sup> concentrations in the pore solution. Equally,

1 CSH in the AAS exhibits different chemical and morphological characteristics compared with PC,  
2 specified with a lower Ca/Si ratio, higher incorporation of Na<sup>+</sup> and substitution of Al<sup>3+</sup> for Si<sup>4+</sup> [59,  
3 73]. This means the conductivity of hydration products in AAS can vary greatly according to the  
4 activator alkalinity and the means through which the alkalis are incorporated into the hydration  
5 products. In this study, sodium silicate gels with a lower Ca/Si ratio, where some of the Si<sup>4+</sup> is  
6 substituted by Al<sup>3+</sup> and Na<sup>+</sup>, could play either a charge balancing role or be absorbed into the CSH  
7 structure. Hence, the current movements in AAS samples could be accelerated. This is in contrast to  
8 PC systems, where hydration products have a relatively insignificant contribution to conductivity [64].  
9 Against this, the electrical conductivity of AAS is much higher than PC at early ages and with  
10 increasing time the solid phases and pore tortuosity increases, leading to electrical conductivity  
11 decreases [46, 74]. These findings agree well with findings in our previous results [17] and other  
12 researchers [74,75].

13 The second contributing feature is that W/B ratio serves as the key factor affecting the  
14 conductivity of both AAS and PC mixes. More liquid will be present in a given sample as its W/B ratio  
15 increases, which in turn will result in higher conductivity [76, 77]. In the case of AAS, increasing W/B  
16 ratio also restricts the concentration of alkali-ions as the total amount of alkali content is kept constant  
17 [78, 79]. Thus, the degree of hydration for AAS with a high W/B ratio diminishes, leading to coarse  
18 pores, higher porosity and, therefore, higher conductivity [80].

19 It is well established that the bulk electrical conductivity itself does not adequately represent  
20 pore structure characteristics of porous materials, although the relative rate of hydration can be  
21 accessed using this parameter. To fully interpret this data, it is necessary to additionally consider pore  
22 solution conductivity. **Figure 4 (b)** shows the conductivity of pore solution extracted from the  
23 hardened paste samples. It is apparent that for a given W/B ratio, the pore solution conductivity of  
24 AAS was much higher than that observed in PC samples. Due to the differences in pore solution  
25 between AAS and PC, it is not surprising to observe this feature, as the pore solution in AAS contains  
26 a high concentration of alkali metal cations and hydroxide ions, which is significantly higher than the  
27 PC samples, resulting in high conductivity [10, 81-83]. It is also apparent that, in comparison to the  
28 PC samples, the bulk conductivity of the AAS samples appeared to vary somewhat with curing  
29 duration; albeit that prolonged curing led to decreasing conductivity of the pore solution. For PC  
30 samples, alkali concentrations (Na<sup>+</sup> and K<sup>+</sup>) increase during the first few days reflecting decreasing  
31 amounts of liquid water, and then stabilise to form hydration products including CSH gel, AFm, AFt  
32 and calcium hydroxide [27, 84, 85]. For AAS systems, hydration reaction is virtually between the slag  
33 particles and the alkali solution, and the initial ion concentration remains extremely high [64, 71, 72].  
34 As GGBS continues to hydrate, the ions in the alkali solution keep reacting with the slag and combining  
35 with the hydration products. The sodium silicate solution provides the essential [SiO<sub>4</sub>]<sup>2-</sup> and Na<sup>+</sup> in C-  
36 (N)-A-S-H gel, yielding large and rapid changes in the ion concentration in pore solution [81, 86]. A  
37 strong dependence of W/B ratio 0.50 AAS over the first 7 days provides further evidences of hydration

1 in AAS, as a low concentration of alkali-activator cannot initiate early polymerisation. Corresponding  
2 delayed hydration processes were also confirmed by the compressive strength results in **Figure 2**.

3 In addition, from **Figure 4 (b)** it is clear that the conductivity of pore solution is inversely  
4 proportional to the W/B ratio for both AAS and PC samples. This trend correlates well with the  
5 variation of ion concentration caused by W/B ratio.

### 6 **4.1.3 Pore size distribution**

7 Cumulative pore volumes for AAS and PC samples at different ages (3, 7 and 28 days), as measured  
8 by MIP, are provided in **Figures 5(a)** and **(c)** respectively. In order to identify pore structure variations,  
9 pores were classified into size categories <10, 10-150 and >50 nm as shown in **Figure 5(c)**. It can be  
10 seen that cumulative volumes of mercury intruded (porosity) for both AAS and PC samples decreased  
11 as the curing duration increased, and both paste types had similar 28-day cumulative pore volumes.  
12 Further, another three interesting features can be identified: 1) from 3 to 7 days, pores becomes finer,  
13 especially for those between 5 and 20 nm, while the overall porosity did not change significantly; 2)  
14 between 7 and 14 days an overall decrease in porosity was found, especially for pores of 10 nm; 3)  
15 from 14 to 28 days the overall porosity was roughly the same and the pores become finer, particularly  
16 for pores between 4 and 8 nm.

17 From early ages, uniform gels fill initially water-filled spaces in AAS and the material gradually  
18 densifies as reactions proceed. In comparison to AAS, pores in PC systems start at around 100 nm,  
19 which are much coarser than that for AAS. With that said, no significant variations in porosity between  
20 AAS and PC samples were found beyond 14 days. The main change occurred in the 2-50 nm pore  
21 range, while no reduction of pores between 50 and 100 nm was found at the age of 28 days. The data  
22 sets in **Figure 5** clearly demonstrate that PC systems have a continuous pore size distribution within  
23 the range 5 to 1000 nm at 28 days, whereas AAS systems predominantly contain pores either in the  
24 <10 or greater than 200 nm ranges. This indicates that in terms of microstructure, AAS systems have  
25 a much denser pore structure, albeit that their total porosity within the capillary range studied are  
26 similar to PC systems. Existence of increased amounts of smaller pores is related to the fact that no  
27 visible inner product ring formation occurs in AAS systems, but rather a dense mass matrix that leads  
28 to high strengths, as shown in **Figure 2**.

29 The peak in the differential pore volume-pore size relationship suggests where the critical  
30 (percolating) pore size is in the system. It should be clarified that the indication of threshold pore  
31 diameter is ideally not an absolute value, but a parameter to facilitate comparisons between specimens,  
32 and which can also be derived from the differential pore volume-pore diameter relationships [87-90].  
33 Beneath this size, the pore system will be de-percolated and, hence, this parameter is very useful for  
34 assessing transport properties [31, 34, 91]. A comparison of threshold pore sizes between AAS and PC  
35 systems is shown in **Table 2**. Clearly, the critical pore radii for AAS-0.35 samples are considerably  
36 smaller than for PC-0.35 samples. It was also found that both AAS and PC systems have shown a

1 decreasing trend as curing duration increased and barely any variation can be detected in the threshold  
2 pore diameter after 14 days, suggesting that the microstructure is less affected beyond this point.  
3 Further investigation into pore structure characteristics for AAS and PC was focused on examining the  
4 influence of W/B ratio. **Figure 6** compares the 28-day MIP results for AAS and PC samples at W/B  
5 ratios 0.35 and 0.50. It can be observed from **Figure 6** that porosity and pore size distribution are  
6 significantly affected by W/B ratio and binder type, with higher porosity and coarser pores associated  
7 with the higher W/B ratio AAS and PC samples.

8 Another noteworthy feature is that the porosity of the AAS samples increased from 22.9 to 44.2%  
9 as the W/B ratio increased from 0.35 to 0.50. Analysis of pore size distribution for AAS-0.50 samples  
10 highlights a marked increase in the number of pores with diameters between 10 and 100 nm, while the  
11 number of fine pores (diameter between 2 and 10 nm) remained similar to the AAS-0.35 samples.  
12 Moreover, the 28-day porosity of AAS-0.50 samples was much higher than the reference PC samples.  
13 A continuous pore size distribution over the measured 2-1000 nm range was detected for AAS-0.50  
14 samples, while only <10 nm pores were observed in the reference PC samples.

15 As explained before, an increase in W/B ratio dilutes the activator concentration which slows  
16 the hydration action rate and precludes high strength at very early ages (lower strength at 3 days for  
17 both AAS samples compared to PC equivalents). Combined with the above AAS-0.35 findings where  
18 AAS samples were found to have a fine pore structure albeit similar porosity compared with reference  
19 PC samples, it can be concluded that W/B ratio plays a more profound role in microstructure formation  
20 for AAS than for PC systems.

## 21 *4.2 Estimation of property variation using microstructural characteristics*

### 22 **4.2.1 Pore formation factor and chloride diffusion coefficient**

23 Pore formation factors and chloride diffusion coefficients were assessed using **Eq (2)** and **(3)** and the  
24 corresponding results are plotted in **Figure 7**. For both AAS and PC samples, the pore formation factor  
25 increased over the entire curing period considered, reflecting the fact that as capillary pores decrease  
26 in volume and size, they start to disconnect because of increases of hydration products [4, 27]. Another  
27 interesting point is that the performance of AAS samples was strongly dependent on W/B ratio. AAS-  
28 0.35 samples returned similar or even lower pore formation factors than corresponding PC samples,  
29 but a much higher value was found when W/B ratio increased to 0.50. Several reasons can be employed  
30 to explain this phenomenon, including the amount of reaction products and difference in pore  
31 structures. The MIP results shown in **Figure 6** suggest that the AAS-0.35 samples produced a denser  
32 microstructure. A comparative analysis of previously obtained SEM results indicate that the hydration  
33 products in AAS are amorphous and uniformly distributed throughout space inside specimens [92, 93].  
34 Thus, it is perhaps not surprising to obtain high formation factors for AAS-35 samples. However, this  
35 is not always valid for the mix with high W/B ratio. This is partially attributed to differences in porosity  
36 variation, as shown in **Figure 3**, and partially because of pore connectivity ( $\beta$  in **Eq (1)**) [41, 94, 95].

1 A detailed analysis of this phenomenon has been presented in a previous related study [78]. It is also  
2 evident in **Figure 7** that AAS samples exhibited different behaviour in the changing rate of pore  
3 formation factor compared with PC, which is affected by the W/B ratio. The pore formation factor for  
4 AAS samples still had not stabilised after 28 days, whereas for PC samples no significant variation  
5 was detected after 7 days. This discrepancy clearly reflects differences in the chemical reactions  
6 occurring in AAS and PC systems

7 **Figure 8** shows the chloride diffusion coefficients determined using the pore formation factor  
8 via **Eq (3)**. As expected, diffusion coefficients for AAS and PC samples and their evolution over the  
9 curing period were generally similar; consistently decreasing with increasing curing duration. AAS  
10 pastes were clearly more sensitive to changing W/B ratio, with only minor decreases in chloride  
11 diffusion observed for the AAS-0.35 samples and no significant variations observed after 14 days. In  
12 contrast, the AAS-0.50 samples exhibited more significant and constant decreases in chloride diffusion  
13 coefficient over 28 days. For the PC samples, at both W/B ratios the diffusion coefficients stabilised  
14 after 7 days. This observation shows consistency with results obtained from other researchers [74, 96]  
15 and is similar to the influence of the pore formation factor explained above.

16 According to work published by McCarter et al [97], more in-depth analysis can predict temporal  
17 variations of chloride diffusion coefficient, with the following equation applied to model obtained  
18 diffusion coefficients at time  $t$  (in days), denoted by  $D_i(t)$ :

$$19 \quad D_i(t) = C \times \left(\frac{D_o}{F_{ref}}\right)^n \times \left(\frac{t_{ref}}{t}\right)^m \quad \text{Eq 10}$$

20 where:  $C$ ,  $n$  and  $m$  are constants;  $D_o$  is the diffusion coefficient of the ion (e.g.  $\text{Cl}^-$ ) in the free  
21 electrolyte at  $25^\circ\text{C}$ ,  $2.03 \times 10^{-9} \text{ m}^2/\text{s}$ ;  $F_{ref}$  is the formation factor at a reference time (d);  $t_{ref}$  is the  
22 reference time in days; and  $m$  is an exponent related to hydration and pozzolanic reactions. The  
23 reference time for the current work was taken as 3 days ( $t_{ref} = 3$  days) and  $F_{ref}$  values are as shown in  
24 **Figure 8**. The three unknown numbers were obtained through multi-parameter nonlinear regression  
25 analysis. During analysis of the diffusion coefficient results, three factors needed to be taken into  
26 account; namely the influence of ions in pore solution, the pore geometry and the binding capacity of  
27 hydration products [96, 98, 99]. These are discussed further in the following paragraph.

28 For AAS systems, more ions are inherently present in the pore solution. In particular,  $\text{Na}^+$  ions  
29 are easily leached from specimens during their service life [100]. Within this process, negatively  
30 charged ions would naturally move to maintain electro neutrality; a process that potentially could slow  
31 down  $\text{Cl}^-$  ion ingress into the specimen. The second factor to be considered are the microstructural  
32 differences between AAS and PC systems. It has been reported [67, 101, 102] that microcracks  
33 frequently occur within AAS-based materials, with the shape of pores reflecting the oval to slot like  
34 shape of microcracks. The results indicate that it is unlikely for AAS systems with a W/B ratio of 0.50  
35 to reach the de-percolation threshold under the exposed curing conditions due to limited hydration.

1 Lastly, differences in physical and chemical binding between PC and AAS systems is the third factor  
2 that requires attention. Established results [58,75,68] have shown that the binding capacity of AAS  
3 samples is much higher than for those made with PC due to a lower Ca/Si ratio and relatively higher  
4 Al content; characteristics beneficial to resist chloride ingress. Therefore, it is reasonable to observe  
5 different regression constants for both AAS and PC samples.

6 To verify the reliability of the proposed equation, correlations between calculated and measured  
7 chloride diffusion coefficients for AAS and PC samples at different curing durations were compared  
8 (see **Figure 9**). As exhibited, a strong correlation was found at different ages, despite the  
9 aforementioned additional influences of ions in pore solution, pore geometry and binding capacity of  
10 hydration products [67, 96, 98-102]. As such, the evaluation of diffusion coefficients using this  
11 methodology was concluded to provide a good estimate of likely performance in practice.

#### 12 **4.2.2 Permeability coefficient**

13 Plotted in **Figure 10** are permeability coefficients for W/B 0.35 mixes estimated using the Katz-  
14 Thomason (KT) and Millington-Quirk (MQ) models according to **Equations (4)** and **(5)** respectively.  
15 Clearly, permeability coefficients for both AAS and PC samples generally reduced gradually over  
16 curing time. For both sample types the majority of reductions occurred during the first 14 days, after  
17 which performance stabilised. This finding agrees with the outputs of previous research [28, 103] and  
18 may be justified due to the fact that variation of permeability is related to the pore structure of reaction  
19 products and pore connectivity. As previously noted, for both PC and AAS samples beyond 14 days  
20 there was no significant variation in porosity (see **Figure 3**), pore structure (see **Figure 5**), critical pore  
21 size (see **Table 2**) or formation factor (see **Figure 8**). The key feature evident from **Figure 10** is that  
22 the AAS samples exhibited significantly better performance in terms of permeability than the PC at  
23 W/B ratio 0.35.

24 No constant conclusion can be drawn from previous studies as conflicting results in this regard  
25 are reported in the literature. Davidovits [104] found the permeability of PC system to be  $10^{-12}$  m/s  
26 ( $10^{-19}$  m<sup>2</sup>) in comparison to  $10^{-11}$  m/s ( $10^{-18}$ m<sup>2</sup>), i.e. one order higher, for alkali-activated materials.  
27 Sagoe-Crentsil *et al* [105] studied the water and gas permeability of AAS and PC concrete and found  
28 that while gas permeability of AAS and PC were similar ( $6.19 \times 10^{-17}$  and  $6.32 \times 10^{-17}$  m<sup>2</sup> respectively),  
29 AAS showed a 10-fold increase in water permeability ( $1.56 \times 10^{-17}$  versus  $1.77 \times 10^{-18}$ m<sup>2</sup>). In previous  
30 work related to this study [67], sorptivity and air permeability were studied and it was found that AAS  
31 concrete exhibited much higher sorptivity and air permeability for a given compressive strength grade.  
32 On the other hand, Zhang *et al.* [106] and Nasvi *et al* [107, 108] conducted measurements of  
33 permeability for AAS concrete and reported lower values than those for PC concrete. Similar findings  
34 were also reported by Ko *et al* [109].

35 Paste AAS and PC samples have a primary porosity different to mixes comprising aggregates  
36 (mortar or concrete), which generally exhibit secondary porosity related to interfacial transition zones

1 [110]. As such, permeability results for paste samples should be closely linked with the microstructure  
2 features determined by MIP. The influence of cracks also needs to be considered here. It has been  
3 reported [67, 101, 102, 110] that considerable microcracks have been observed for AAS concrete, and  
4 especially within aggregate-paste interfaces; a phenomenon undoubtedly influencing permeability.  
5 Meanwhile, the variability and properties of raw materials and mix proportions also affects  
6 permeability results. As such, it is not hard to understand opposing trends being reported in the  
7 literature. The observed results in this study highlight the fact that AAS can achieve low permeability;  
8 a finding which has considerable practical significance. However, this cannot be the case for AAS with  
9 high W/B ratios.

10 It is also worth noting that permeability coefficients derived from the two models cannot be equal.  
11 More specifically, permeability coefficients estimated using the KT model are one order lower than  
12 those using the MQ model. The KT model is built on the fact that the rate of flow between two pores  
13 of different sizes is controlled by the pore of the smallest size, or the so-called neck. This presupposes  
14 a perfect fit between the two pores, which rarely exists in reality. It is assumed that the pores and necks  
15 are circular in cross section, although it is shown that they have a rather angular shape [30, 31]. Also,  
16 another assumption is that only one neck arises in sequence with another neck in the same pore. Errors  
17 generated from these assumptions at least partially offset against other errors by neglecting the  
18 widening pores. The threshold pore method used in the KT model does permit a rather rapid calculation  
19 of permeability, but the accuracy and reliability of this model should be questioned. As shown in this  
20 study, the KT model could give misleading results when assessing the permeability of AAS with a  
21 W/B ratio of 0.50. **Figure 11** shows the estimated 28-day permeability values for AAS and PC samples  
22 with W/B ratios 0.35 and 0.50. It can be seen that the two models yielded a higher permeability  
23 coefficient as the W/B ratio increases, but a different trend was obtained when the W/B ratio was 0.50.  
24 In other words, AAS is less permeable than PC in the case of KT model, while an opposite conclusion  
25 is given if the MQ model is applied. As indicated in the above section, AAS with high W/B ratio has  
26 a coarse and continuous pore structure and high porosity, which would yield a higher permeability  
27 coefficient. Therefore, it may be concluded that the KT model may not be suitable for estimating the  
28 permeability of AAS, as only threshold diameter considerations do not fully represent the complexity  
29 of its pore structure in reality.

### 30 **4.2.3 Compressive strength**

31 In **Figure 12**, the porosity of AAS and PC samples is plotted against compressive strength. It can be  
32 seen that all pastes are porous bodies with porosities ranging between about 20% and 55%. As porosity  
33 levels mainly originate from the fraction of mixing liquids, it is expected that increasing compressive  
34 strength is a consequence of porosity and W/B ratio decreasing. Considering the variability of the data,  
35 the relationships between two parameters is good. Furthermore, a general trend between compressive  
36 strength and porosity can be found for AAS and PC samples. This is easy to understand because the

1 strength of both binders comes from the CSH [111, 112], although the ratio of crystalline and Ca/Si in  
2 these hydration products is different. The four strength-porosity relationships discussed in section 2.4  
3 were used to predict the experimental results, where non-linear regression analysis was applied to  
4 obtain the coefficients for AAS and PC in **Eq (6-1)** to **Eq (6-4)**. From **Figure 12** it is clear that the  
5 correlation coefficients of regression constants ranged from 0.662 to 0.948 for the four modules.  
6 Compared to Balshin's and Ryshkevitch's equations, Schiller's and Hasselman's equation appear to  
7 be less accurate. This conclusion differs with some studies, e.g. Shi [91], which has shown an opposite  
8 observation. A possible reason explaining this situation is the type of GGBS used in the different  
9 studies, as it has been shown that GGBS-type dominates responses of AAS cement materials. In  
10 addition, different methods used to determine porosity may be another reason for this observation.  
11 Porosity reported in this study was determined at 40 °C (selected to avoid additional changes in  
12 microstructure and hydration products during drying [27, 113, 114]), instead of at 105 °C for the  
13 aforementioned study.

## 14 **5. Conclusion**

15 In this study, the microstructural characteristics and electrical responses were used to assess and predict  
16 the performance of AAS cement. The compressive strength, permeable porosity, bulk conductivity,  
17 pore solution conductivity and pore structure of AAS and corresponding reference PC paste samples  
18 were measured. Based on the results obtained, and following conclusions can be drawn:

- 19 1. It has been found that classical theories used for predicting the performance of PC through  
20 microstructural characteristics and electrical responses can be applied to assess AAS cement. Pore  
21 formation factor, chloride diffusivity and permeability were estimated along with an evaluation of  
22 different porosity-compressive strength models
- 23 2. The results show that the chloride transport coefficient can be reliably predicted using electrical  
24 responses. According to the regression analysis, no empirical equation can be established between  
25 AAS cement and PC, and hence it is recommended to establish an equation for the material for  
26 the specific condition.
- 27 3. Previous studies have highlighted that the AAS cement has refined pore structure with a relatively  
28 narrow pore size distribution. It is found that the general trend is only valid when the W/B ratio is  
29 low, while this feature cannot be observed for the cement paste with a high W/B ratio. It suggests  
30 that the assumption of AAS will have a denser pore structure than that of PC for a given W/B is  
31 not safe.
- 32 4. Analysis of temporal variation of formation factor indicates that the AAS cement has a relatively  
33 constant growth rate until 28 days, while the formation factor of PC intends to increase rapidly  
34 before 7 days and after this, the variation is relatively small. This feature highlights the importance  
35 of continuous curing for AAS cement, as normal curing regime for PC would not be sufficient to

1 ensure its quality. Meanwhile, the high sensitivity to the W/B ratio is clearly seen from the  
2 performance range obtained. It means that AAS has the potential to achieve super durability, but  
3 this binding system would require more care on manufacturing techniques.

## 4 **Acknowledgement**

5 The experiments described in this paper were carried out at Chongqing University. The authors  
6 acknowledge the following institutions for providing facilities and the financial support: National  
7 Natural Science Foundation of China (NO. 51878102), Open funds from Shenzhen University, State  
8 Key Laboratory of High Performance Civil Engineering Materials, Chongqing Jiaotong University,  
9 Venture and innovation support program for Chongqing oversea returns. In addition, support provided  
10 from University of Leeds and Ulster University during analysis of data and preparation of this paper  
11 are also highly appreciated.

## 12 **References**

- 13 [1] Xu D, Cui Y, Li H, Yang K, Xu W, Chen Y. On the future of Chinese cement industry. *Cement*  
14 *and Concrete Research*. 2015;78:2-13.
- 15 [2] Dewar JD, Dhir RK, Abernethy I, Adler D, Bamforth PB, Corish AT, et al. *The use of GGBS and*  
16 *PFA in concrete*. Slough: Concrete Society; 1991. p. 145.
- 17 [3] Ludwig H-M, Zhang W. Research review of cement clinker chemistry. *Cement and Concrete*  
18 *Research*. 2015;78:24-37.
- 19 [4] Taylor HF. *Cement chemistry*: Thomas Telford; 1997.
- 20 [5] Sekiguchi N. *Steel market developments: 2<sup>nd</sup> Quarter 2015*. Paris: OECD; 2015. p. 25.
- 21 [6] Basson E. *World steel in figures*. Lyon, France: World Steel Association; 2016. p. 30.
- 22 [7] Albitar M, Mohamed Ali MS, Visintin P, Drechsler M. Durability evaluation of geopolymers and  
23 conventional concretes. *Construction and Building Materials*. 2017;136:374-85.
- 24 [8] Frank C, J.G. S. Effect of pore size distribution on drying shrinkage of alkali-activated slag  
25 concrete. *Cement and Concrete Research*. 2000;30:1401-6.
- 26 [9] Wang SD, Pu XC, Scrivener K, Pratt PL. Alkali-activated slag cement and concrete: A review of  
27 properties and problems. *Advances in Cement Research*. 1995;27:93-102.
- 28 [10] Bernal SA, Provis JL, Green DJ. Durability of Alkali-Activated Materials: Progress and  
29 Perspectives. *Journal of the American Ceramic Society*. 2014;97(4):997-1008.
- 30 [11] Duxson P, Provis JL, Lukey GC, van Deventer JSJ. The role of inorganic polymer technology in  
31 the development of 'green concrete'. *Cement and Concrete Research*. 2007;37(12):1590-7.
- 32 [12] Roy DM, Jiang W, Silsbee MR. Chloride diffusion in ordinary, blended, and alkali-activated  
33 cement pastes and its relation to other properties. *Cement and Concrete Research*. 2000;30:1879-  
34 84.
- 35 [13] Chi M. Effects of modulus ratio and dosage of alkali-activated solution on the properties and  
36 micro-structural characteristics of alkali-activated fly ash mortars. *Construction and Building*  
37 *Materials*. 2015;99:128-36.

- 1 [14] Aydın S, Baradan B. Mechanical and microstructural properties of heat cured alkali-activated slag  
2 mortars. *Materials & Design*. 2012;35:374-83.
- 3 [15] Yi YL, Li C, Liu SY. Alkali-activated ground granulated blast furnace slag for stabilisation of  
4 marine soft clay. *Journal of Materials in Civil Engineering*. 2014.
- 5 [16] Brandão Ferreira LF, Coelho JFJ, Antunes Barata II, Sousa Costa HS, Tiago PMN, Júlio ENBS.  
6 Precast alkali-activated concrete towards sustainable construction. *Magazine of Concrete*  
7 *Research*. 2014;66(12):618-26.
- 8 [17] Yang K, Yang C, Zhang J, Pan Q, Yu L, Bai Y. First structural use of site-cast, alkali-activated  
9 slag concrete in China. *Proceedings of the Institution of Civil Engineers - Structures and*  
10 *Buildings*. 2017:1-10.
- 11 [18] Buchwald A, Vanooteghem M, Gruyaert E, Hilbig H, Belie ND. Purdocement-Application of  
12 alkali-activated slag cement in Belgium in the 1950s. *Materials and Structures*. 2013.
- 13 [19] Zhang Z, Li L, Ma X, Wang H. Compositional, microstructural and mechanical properties of  
14 ambient condition cured alkali-activated cement. *Construction and Building Materials*.  
15 2016;113:237-45.
- 16 [20] Palacios M, Puertas F. Effect of superplasticizer and shrinkage-reducing admixtures on alkali-  
17 activated slag pastes and mortars. *Cement and Concrete Research*. 2005;35:1358-67.
- 18 [21] Bilek Jr V, Kalina L, Tkacz J, Parizek L. Some issues of shrinkage-reducing admixtures  
19 application in alkali-activated slag systems. *Materials*. 2016;462(9):1-12.
- 20 [22] Collins F, Sanjayan JG. Cracking tendency of alkali-activated slag concrete subjected to restrained  
21 shrinkage. *Cement and Concrete Research*. 2000;30:791-8.
- 22 [23] Ye H, Radlińska A. Shrinkage mechanisms of alkali-activated slag. *Cement and Concrete*  
23 *Research*. 2016;88:126-35.
- 24 [24] Azarsa R, Gupta R. Electrical resistivity of concrete for durability evaluation: A review. *Advances*  
25 *in Materials Science and Engineering*, <https://doi.org/10.1155/2017/8453095>, 2017: 30 pages.
- 26 [25] Lee SH, Rasaiah JC. Molecular dynamics simulation of ionic mobility. I. Alkali metal cations in  
27 water at 25 °C. *The Journal of Chemical Physics*. 1994;101(8):6964-74.
- 28 [26] Lee SH, Rasaiah JC. Molecular dynamics simulation of ion mobility. 2-Alkali metal and halide  
29 ions using the SPCE model for water at 25 °C. *The Journal of Chemical Physics*. 1996;100:1420-  
30 5.
- 31 [27] Neville AM. *Properties of concrete*. 4<sup>th</sup> ed: Pearson; 1995.
- 32 [28] Basheer PAM. Permeation analysis. In: V.S. R, Beaudoin JJ, editors. *Handbook of Analytical*  
33 *Techniques in Concrete Science and Technology: Principles, Techniques and Applications*: Noyes  
34 *Publications*; 2001. p. 658-727.
- 35 [29] Carman PC. *Fluid flow through granular beds*. 1937.
- 36 [30] Dullien FAL. *Porous media: Fluid transport and pore structure*. San Diego, California: Academic  
37 *Press*; 1992.
- 38 [31] Bear J. *Dynamics of fluid in porous media*. New York: American Elsevier; 1972.
- 39 [32] Ma H. Mercury intrusion porosimetry in concrete technology: tips in measurement, pore structure  
40 parameter acquisition and application. *J Porous Mater*. 2013;21(2):207-15.
- 41 [33] Katz A, Thompson AH. Quantitative prediction of permeability in porous rock. *Physical Review*  
42 *B*. 1986;34:8179-81.

- 1 [34] Nokken MR, Hooton RD. Using pore parameters to estimate permeability or conductivity of  
2 concrete. *Materials and Structures*. 2007;41(1):1-16.
- 3 [35] Millington RJ, Quirk JP. Formation factor and permeability equations. *Nature*. 1964;202:143-5.
- 4 [36] Bentz D, Quenard DA, Kunzel HM, Baruchel J, Peyrin F, Martys NS, et al. Microstructure and  
5 transport properties of porous building materials II Three-dimensional X-ray tomographic studies.  
6 *Materials and Structures*. 2000;33:147-53.
- 7 [37] Cnudde V, Cwirzen A, Masschaele B, Jacobs F. Porosity and microstructure characterization of  
8 building stones and concretes. *Engineering Geology*. 2009;103:76-83.
- 9 [38] Abell AB, Willis KL, Lange A. Mercury Intrusion Porosimetry and Image Analysis of Cement-  
10 Based Materials. *Journal of Colloid and Interface Science*. 1999;211:39-44.
- 11 [39] Diamond S. Mercury porosimetry: An inappropriate method for the measurement of pore size  
12 distributions in cement-based materials. *Cement and Concrete Research*. 2000;30:1517-25.
- 13 [40] Windslow D, Diamond S. A mercury porosimetry study of the evolution of porosity in Portland  
14 cement. Joint highway research report. US: Purdue University; 1969.
- 15 [41] Nokken MR, Hooton RD. Discontinuous capillary porosity in concrete – Does it exist? In: Weiss  
16 J, Kovler K, Marchand J, Mindess S, editors. *International RILEM Symposium on Concrete  
17 Science and Engineering: A Tribute to Arnon Bentur*: RILEM Publications SARL; 2004.
- 18 [42] Mindess S. Relation between the compressive strength and porosity of autoclaved calcium silicate  
19 hydrates. *Journal of the American Ceramic Society*. 1970;53:621-4.
- 20 [43] Odler I, Robler M. Investigations on the relationship between porosity structure and strength of  
21 hydrated Portland cement pastes: II. Effect of pore structure and of degree of hydration. *Cement  
22 and Concrete Research*. 1985;15:401-10.
- 23 [44] Roy DM, Gouda GR. Porosity-strength relation in cementitious materials in very high strengths.  
24 *Journal of the American Ceramic Society*. 1973;56:549-50.
- 25 [45] Chen XD, Wu SX, Zhou JK. Influence of porosity on compressive and tensile strength of cement  
26 mortar. *Construction and Building Materials*. 2013;40:869-74.
- 27 [46] Yang K, Basheer PAM, Magee BJ, Bai Y. Investigation of moisture condition and Autoclam  
28 sensitivity on air permeability measurements for both normal concrete and high performance  
29 concrete. *Construction and Building Materials*. 2013;48:306-14.
- 30 [47] Jennings HM, Bullard JW, Thomas JJ, Andrade JE, Chen JJ, Scherer GW. Characterization and  
31 modeling of pores and surfaces in cement paste: Correlations to processing and properties. *Journal  
32 of Advanced Concrete Technology*. 2008;6(1):5-29.
- 33 [48] Rusin Z, Świercz P. Volumetric strains of cement-based mortars caused by ice formation in terms  
34 of frost resistance diagnostics. *Bulletin of the Polish Academy of Sciences Technical Sciences*.  
35 2015;63:35-41.
- 36 [49] Medeiros-Junior RA, Lima MG. Electrical resistivity of unsaturated concrete using different types  
37 of cement. *Construction and Building Materials*. 2016;107:11-6.
- 38 [50] Wei X, Xiao L. Electrical resistivity monitoring and characterisation of early age concrete.  
39 *Magazine of Concrete Research*. 2013;65(10):600-7.
- 40 [51] Vollpracht A, Lothenbach B, Snellings R, Haufe J. The pore solution of blended cements: a  
41 review. *Materials and Structures*. 2016;49:3341-67.

- 1 [52] Barneyback RS, Diamond S. Expression and analysis of pore fluids from hardened cement pastes  
2 and mortars. *Cement and Concrete Research*. 1981;11:279-85.
- 3 [53] Ma H, Hou D, Lu Y, Li Z. Two-scale modeling of the capillary network in hydrated cement paste.  
4 *Construction and Building Materials*. 2014;64:11-21.
- 5 [54] Peng ZH, Vance K, Dakhane A, Marzke R, Neithalath N. Microstructural and <sup>29</sup>Si MAS NMR  
6 spectroscopic evaluations of alkali cationic effects on fly ash activation. *Cement and Concrete*  
7 *Composites*. 2015;57:34-43.
- 8 [55] GB/T-17671. Method of Testing cements-Determination of strength. Beijing: The State Bureau  
9 of Quality and Technical Supervision; 1999. p. 9 pages.
- 10 [56] Ding Y, Dai J-G, Shi C-J. Mechanical properties of alkali-activated concrete: A state-of-the-art  
11 review. *Construction and Building Materials*. 2016;127:68-79.
- 12 [57] Shi C, Day RL. Some factors affecting early hydration of alkali-slag cements. *Cement and*  
13 *Concrete Research*. 1996;26:439-47.
- 14 [58] Wang SD, Scrivener K. Hydration products of alkali activated slag cement. *Cement and Concrete*  
15 *Research*. 1995;25:561-71.
- 16 [59] Gruskovnjak A, Lothenbach B, Holzer L, Figi R, Winnefeld F. Hydration of alkali-activated slag-  
17 Comparison with ordinary Portland cement. *Advances in Cement Research*. 2006;18:119-28.
- 18 [60] Ben Haha M, Le Saout G, Winnefeld F, Lothenbach B. Influence of activator type on hydration  
19 kinetics, hydrate assemblage and microstructural development of alkali activated blast-furnace  
20 slags. *Cement and Concrete Research*. 2011;41(3):301-10.
- 21 [61] Hubler MH, Thomas JJ, Jennings HM. Influence of nucleation seeding on the hydration kinetics  
22 and compressive strength of alkali activated slag paste. *Cement and Concrete Research*.  
23 2011;41(8):842-6.
- 24 [62] Yang LY, Jia ZJ, Zhang YM, Dai JG. Effects of nano-TiO<sub>2</sub> on strength, shrinkage and  
25 microstructure of alkali activated slag pastes. *Cement and Concrete Composites*. 2015;57:1-7.
- 26 [63] Gebregziabihier BS, Thomas R, Peethamparan S. Very early-age reaction kinetics and  
27 microstructural development in alkali-activated slag. *Cement and Concrete Composites*.  
28 2015;55:91-102.
- 29 [64] Ravikumar D, Neithalath N. An electrical impedance investigation into the chloride ion transport  
30 resistance of alkali silicate powder activated slag concretes. *Cement and Concrete Composites*.  
31 2013;44:58-68.
- 32 [65] Bernal SA, de-Gutierrez RM, Provis JL. Engineering and durability properties of concretes based  
33 on alkali-activated granulated blast furnace slagmet. *Construction and Building Materials*.  
34 2012;33:99-108.
- 35 [66] Olivia M, Sarker PK, Nikraz H. Water penetrability of low calcium fly ash geopolymer concrete.  
36 *International Conference Construction Building Technology (ICCBT)2008*. p. 517-30.
- 37 [67] Yang K, Yang C, Magee B, Nanukuttan S, Ye J. Establishment of a preconditioning regime for  
38 air permeability and sorptivity of alkali-activated slag concrete. *Cement and Concrete Composites*.  
39 2016;73:19-28.
- 40 [68] Al-Otaibi S. Durability of concrete incorporating GGBS activated by water glass. *Construction*  
41 *and Building Materials*. 2008;22:2059-67.

- 1 [69] A.R. B, A. A. Sodium silicate-based, alkali-activated slag mortars Part I. Strength, hydration and  
2 microstructure. *Cement and Concrete Research*. 2002;32:865-79.
- 3 [70] Tanzer R, Buchwald A, Stephan D. Effect of slag chemistry on the hydration of alkali-activated  
4 blast-furnace slag. *Materials and Structures*. 2015;48:629-41.
- 5 [71] McCarter J, Starrs G, Chrisp M. Diffusion kinetics in cementitious binders. *Journal of Materials*  
6 *Science Letters*. 2000;19:1279-80.
- 7 [72] Polder R, Peelen WHA. Characterisation of chloride transport and reinforcement corrosion in  
8 concrete under cyclic wetting and drying resistivity. *Cement and Concrete Composites*.  
9 2002;24:427-35.
- 10 [73] Richardson IG, Girão AV, Taylor R, Jia S. Hydration of water- and alkali-activated white Portland  
11 cement pastes and blends with low-calcium pulverized fuel ash. *Cement and Concrete Research*.  
12 2016;83:1-18.
- 13 [74] Ma Q, Nanukuttan SV, Basheer PAM, Bai Y, Yang C. Chloride transport and the resulting  
14 corrosion of steel bars in alkali activated slag concretes. *Materials and Structures*. 2015.
- 15 [75] Rodriguez ED, Bernal SA, Mejia de Gutierrez R, Puertas F. Alternative concrete based on alkali-  
16 activated slag. *Materiales de Construccion*. 2008;58:53-67.
- 17 [76] Farnam Y, Todak H, Spragg R, Weiss J. Electrical response of mortar with different degrees of  
18 saturation and deicing salt solutions during freezing and thawing. *Cement and Concrete*  
19 *Composites*. 2015;59:49-59.
- 20 [77] Wang Y, Nanukuttan S, Bai Y, Basheer PAM. Influence of combined carbonation and chloride  
21 ingress regimes on rate of ingress and redistribution of chlorides in concretes. *Construction and*  
22 *Building Materials*. 2017;140:173-83.
- 23 [78] John L. P, Rupert J. M, Claire E. W, Volker R, Jannie S.J. V-D. X-ray microtomography shows  
24 pore structure and tortuosity in alkali-activated binders. *Cement and Concrete Research*.  
25 2012;42:855-64.
- 26 [79] Ismail I, Bernal SA, Provis JL, Hamdan S, van Deventer JSJ. Drying-induced changes in the  
27 structure of alkali-activated pastes. *Journal of Materials Science*. 2013;48(9):3566-77.
- 28 [80] Zhang M, Zhao M, Zhang G, El-Korchi T, Tao M. A multiscale investigation of reaction kinetics,  
29 phase formation, and mechanical properties of metakaolin geopolymers. *Cement and Concrete*  
30 *Composites*. 2017;78:21-32.
- 31 [81] Lloyd RR, Provis JL, van Deventer JSJ. Pore solution composition and alkali diffusion in  
32 inorganic polymer cement. *Cement and Concrete Research*. 2010;40(9):1386-92.
- 33 [82] Puertas F, Fernández-Jiménez A, Blanco-Varela MT. Pore solution in alkali-activated slag cement  
34 pastes. Relation to the composition and structure of calcium silicate hydrate. *Cement and Concrete*  
35 *Research*. 2004;34(1):139-48.
- 36 [83] Rothstein D, Thomas JJ, Cristensen BJ, Jennings HM. Solubility behavior of Ca-, S-, Al-, and Si-  
37 bearing solid phases in Portland cement pore solution as a function of hydration time. *Cement and*  
38 *Concrete Research*. 2002;32:1663-71.
- 39 [84] Mehta PK, Monteiro PJM. *Concrete: Microstructure, Properties, and Materials*. 3<sup>rd</sup> ed: McGraw-  
40 Hill Professional; 2005.

- 1 [85] Lecomte I, Henrist C, Liégeois M, Maseri F, Rulmont A, Cloots R. (Micro)-structural comparison  
2 between geopolymers, alkali-activated slag cement and Portland cement. *J Eur Ceram Soc.*  
3 2006;26(16):3789-97.
- 4 [86] Ogirigbo OR, Black L. Influence of slag composition and temperature on the hydration and  
5 microstructure of slag blended cements. *Construction and Building Materials.* 2016;126:496-507.
- 6 [87] Cook RA, Hover KC. Mercury porosimetry of cement-based materials and associated correction  
7 factors. *Construction and Building Materials.* 1993;7:231-40.
- 8 [88] Diamond S. The microstructure of cement paste and concrete-a visual primer. *Cement and*  
9 *Concrete Composites.* 2004;26(8):919-33.
- 10 [89] Cook RA, Hover KC. Mercury porosimetry of hardened cement pastes. *Cement and Concrete*  
11 *Research.* 1999;29:933-43.
- 12 [90] Atahan HN, Oktar ON, Tasdemir C. Effects of water-cement ratio and curing time on the critical  
13 pore width of hardened cement paste. *Construction and Building Materials.* 2009;23:1196-200.
- 14 [91] Shi C. Strength, pore structure and permeability of alkali-activated slag mortars. *Cement and*  
15 *Concrete Research.* 1996;26:1789-99.
- 16 [92] Lloyd RR, Provis JL, van Deventer JSJ. Microscopy and microanalysis of inorganic polymer  
17 cements. 2: the gel binder. *Journal of Materials Science.* 2008;44(2):620-31.
- 18 [93] Gebregziabihher BS, Thomas RJ, Peethamparan S. Temperature and activator effect on early-age  
19 reaction kinetics of alkali-activated slag binders. *Construction and Building Materials.*  
20 2016;113:783-93.
- 21 [94] Sant G, Bentz D, Weiss J. Capillary porosity depercolation in cement-based materials:  
22 Measurement techniques and factors which influence their interpretation. *Cement and Concrete*  
23 *Research.* 2011;41(8):854-64.
- 24 [95] Suryanto B, Saraireh D, Kim J, McCarter WJ, Starrs G, Taha HM. Imaging water ingress into  
25 concrete using electrical resistance tomography. *International Journal of Advances in Engineering*  
26 *Sciences and Applied Mathematics.* 2017.
- 27 [96] Ravikumar D, Neithalath N. Electrically induced chloride ion transport in alkali activated slag  
28 concretes and the influence of microstructure. *Cement and Concrete Research.* 2013;47:31-42.
- 29 [97] McCarter WJ, Chrisp TM, Starrs G, Basheer PAM, Nanukuttan S, Srinivasan S, et al. A durability  
30 performance-index for concrete: developments in a novel test method. *International Journal of*  
31 *Structural Engineering.* 2015;6:2-22.
- 32 [98] Tang L, Nilsson LO, Basheer PAM. *Resistance of Concrete to Chloride Ingress: Testing and*  
33 *modelling: Spon Press; 2011.*
- 34 [99] Wong HS, Buenfeld NR, Zobel M, Zimmerman RW. Influence of the interfacial transition zone  
35 and microcracking on the diffusivity, permeability and sorptivity of cement-based materials after  
36 drying. *Magazine of Concrete Research.* 2009;61(8):571-89.
- 37 [100] Shi C, Julia A, Stegemann A, Caldwell RJ. Effect of supplementary cementing materials on  
38 specific conductivity of pore solution and its implications on the rapid chloride permeability test  
39 (AASHTO T277) results. *ACI Materials Journal.* 1998;95:389-94.
- 40 [101] Collins FG, Sanjayan J. Capillary shape: Influence on water transport within unsaturated alkali  
41 activated slag concrete. *Journal of Materials in Civil Engineering.* 2010;22:260-6.

- 1 [102] Zhang Z, Yao X, Zhu H. Potential application of geopolymers as protection coatings for marine  
2 concreteII. Microstructure and anticorrosion mechanism. *Applied Clay Science*. 2010;49(1-2):7-  
3 12.
- 4 [103] NO.31 Tr. Permeability testing of site concrete: A review of methods and experience. *Concrete*  
5 *Society*; 2008. p. 1-80.
- 6 [104] Davidovits J. Properties of geopolymer cements. *International conference on alkaline cements*  
7 *and concretes*. Ukraine1994. p. 131-49.
- 8 [105] Sagoe-Crentsil K, Brown T, Yan S. Medium to long term engineering properties and  
9 performance of high-strength geopolymers for structural applications. *Advances in Science and*  
10 *Technology*. 2010;69:135-42.
- 11 [106] Zhang Z, Yao X, Zhu H. Potential application of geopolymers as protection coatings for marine  
12 concreteI. Basic properties. *Applied Clay Science*. 2010;49(1-2):1-6.
- 13 [107] M. N, P.G. R, J. S. The permeability of geopolymer at down-hole stress conditions: Application  
14 for carbon dioxide sequestration wells. *Applied Engineey*. 2013;102:1391-8.
- 15 [108] Nasvi MCM, Ranjith PG, Sanjayan JG. Effect of different mix compositions on apparent carbon  
16 dioxide (CO<sub>2</sub>) permeability of geopolymer: Suitability as well cement for CO<sub>2</sub> sequestration  
17 wells. *Applied Energy*. 2014;114:939-48.
- 18 [109] Ko M-S, Chen H-Y, Lyu S-J, Wang T-T, Ueng T-H. Permeation characteristics and impact  
19 factors of geopolymers made of kaolin. *Construction and Building Materials*. 2015;93:301-8.
- 20 [110] San Nicolas R, Bernal SA, Mejía de Gutiérrez R, van Deventer JSJ, Provis JL. Distinctive  
21 microstructural features of aged sodium silicate-activated slag concretes. *Cement and Concrete*  
22 *Research*. 2014;65:41-51.
- 23 [111] Feldman RF, Beaudoin JJ. Microstructure and strength of hydrated cement. *Cement and*  
24 *Concrete Research*. 1976;6:389-400.
- 25 [112] Shi C, Krivenko PV, Roy DM. *Alkali-activated cements and concretes*: Taylor and Francis;  
26 2005.
- 27 [113] Yang K. Estimates of concrete transport properties by a two pressure water test. *Magazine of*  
28 *Concrete Research*. 2016;68(10):530-40.
- 29 [114] Parrott LJ. Factors influencing relative humidity in concrete. *Magazine of Concrete Research*.  
30 1991;43:45-52.

31  
32

**Figure and Table**

- 1
- 2 Table 1 Chemical composition of GGBS and PC (% by mass)
- 3 Table 2 Temporal variation of threshold diameter of AAS and PC
- 4 Figure 1 High pressure pore solution extraction device (SBT, CO., LTD.)
- 5
- 6 Figure 2 Compressive strength development of both AAS and PC pastes
- 7 Figure 3 Accessible porosity of AAS and PC pastes
- 8 Figure 4 Plots of bulk and pore solution electrical conductivity of AAS and PC pastes
- 9 Figure 5. Pore size distribution of (a) AAS pastes with W/B ratio of 0.35 at 3 d, 7d, 14d and 28d; (b) PC pastes with
- 10 W/B ratio of 0.35 at 3d, 7d, 14d and 28d; (c) comparison of pore volume ratio of AAS and PC pastes; (d)
- 11 comparison of pore proportion based on the classification in (c).
- 12 Figure 6. Comparison of the pore size distribution of AAS and PC pastes with 0.35 and 0.50 W/B ratios at 28 days
- 13 Figure 7. Temporal variation of formation factor of AAS and PC pastes
- 14 Figure 8. Temporal variation of Cl<sup>-</sup> diffusion coefficient of AAS and PC pastes
- 15 Figure 9 Comparison between the measured Cl<sup>-</sup> diffusion coefficient and estimated Cl<sup>-</sup> diffusion coefficient
- 16 Figure 10 Comparison of estimated permeability coefficients of AAS and PC pastes
- 17 Figure 11 Permeability coefficients of AAS and PC pastes with different W/B ratios estimated by MQ and KT
- 18 models
- 19 Figure 12. Relationship between porosity and compressive strength of AAS and PC pastes
- 20

1

**Table 1** Chemical composition of GGBS and PC (% by mass)

Composition	SiO <sub>2</sub>	Al <sub>2</sub> O <sub>3</sub>	Fe <sub>2</sub> O <sub>3</sub>	MgO	CaO	Na <sub>2</sub> O	K <sub>2</sub> O	Loss
GGBS	31.63	13.42	1.32	9.12	36.35	0.34	0.46	0.61
PC	21.33	5.80	2.57	2.41	60.21	0.70	0.21	--

2

3

**Table 2** Temporal variation of threshold diameter of AAS and PC

Curing duration (day)	AAS-35 (nm)	PC-35 (nm)
3	11.0	62.4
7	9.1	62.4
14	6.0	50.3
28	5.2	50.3

4

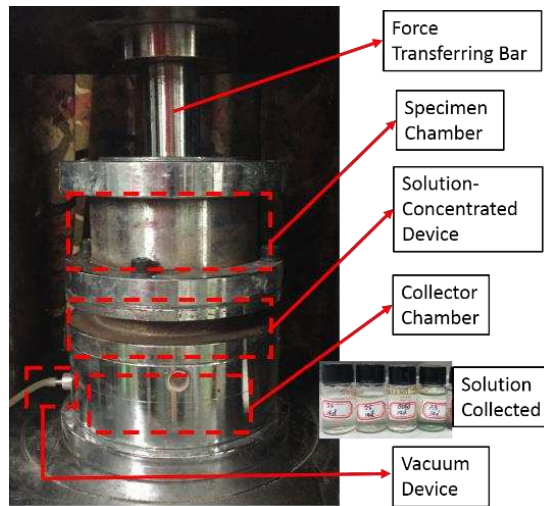


**Figure 1** High pressure pore solution extraction device

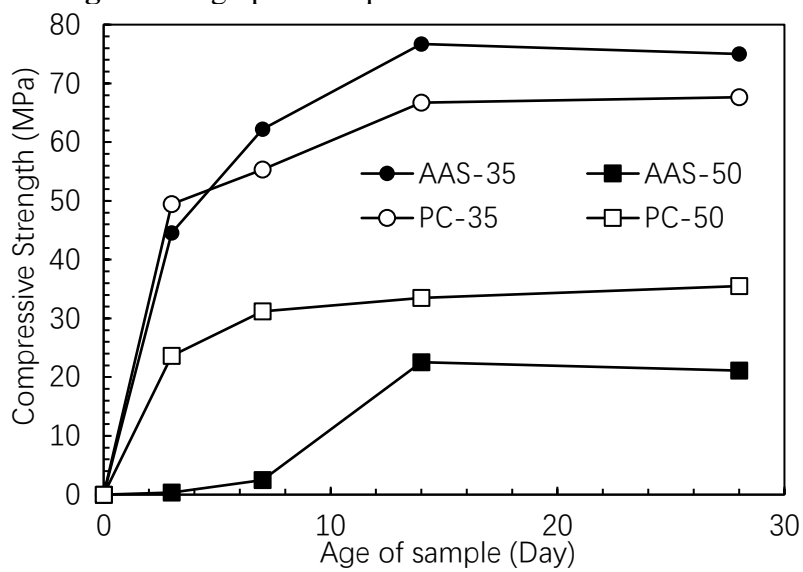


**Figure 2** Compressive strength development of AAS and PC pastes

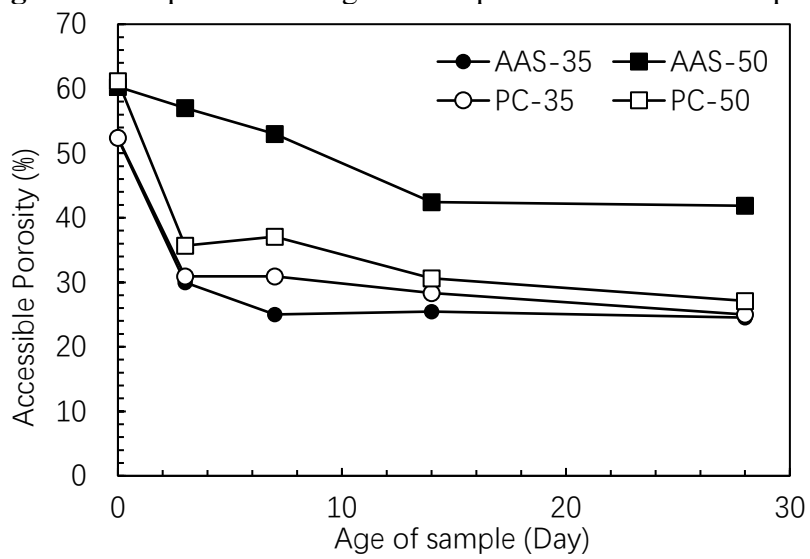
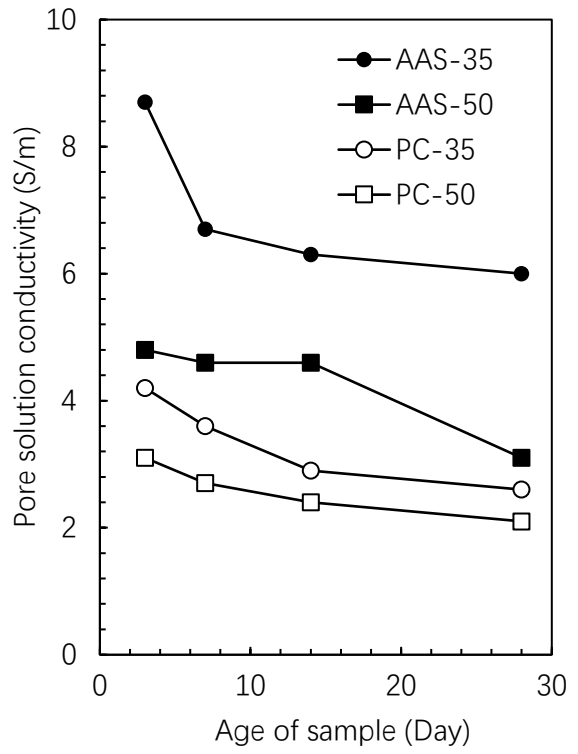
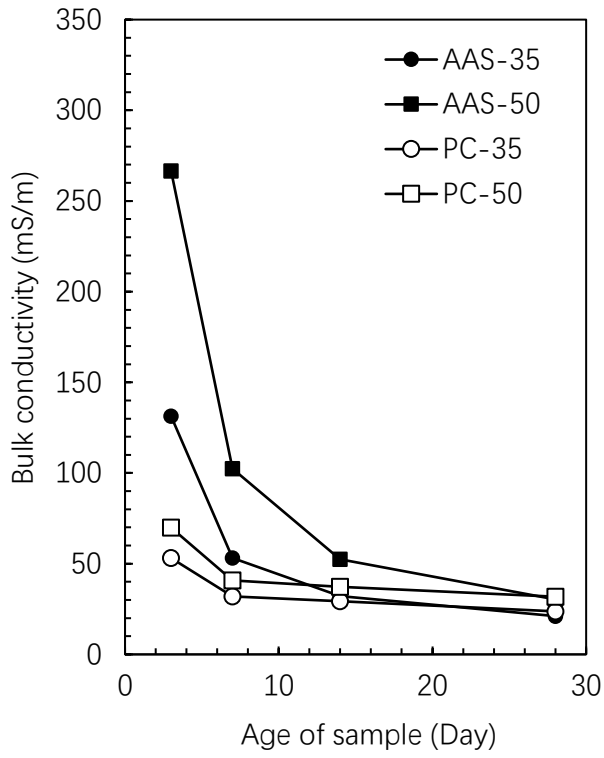


**Figure 3** Accessible porosity of AAS and PC pastes

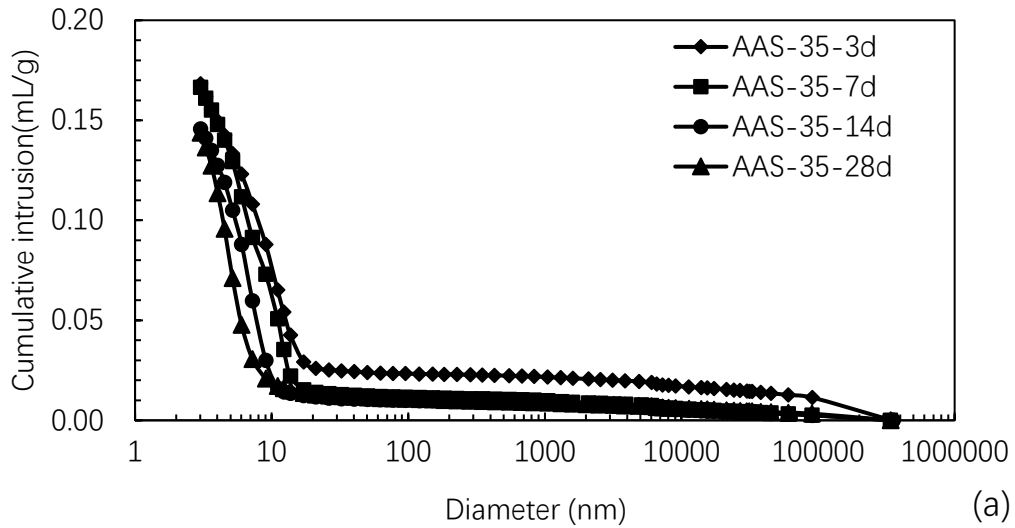


(a) bulk conductivity

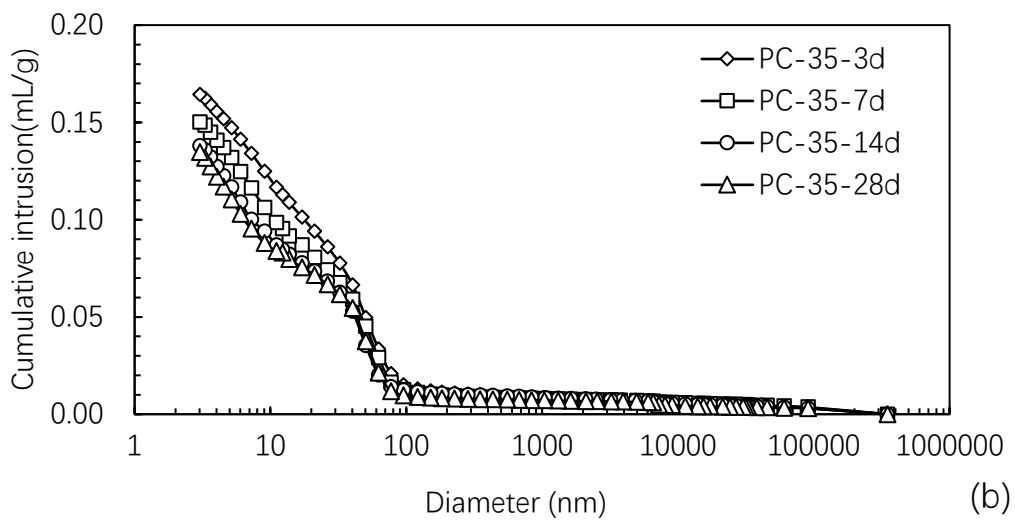
(b) pore solution conductivity

**Figure 4** Plots of bulk and pore solution electrical conductivity of AAS and PC pastes

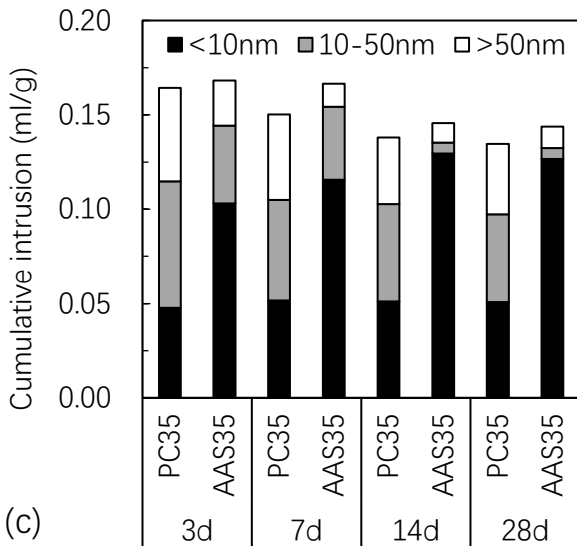
1  
2  
3



1



2



3

4

5

6

7

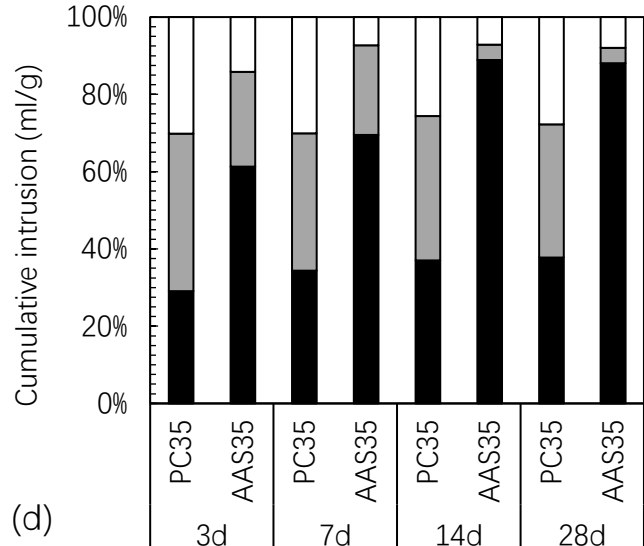
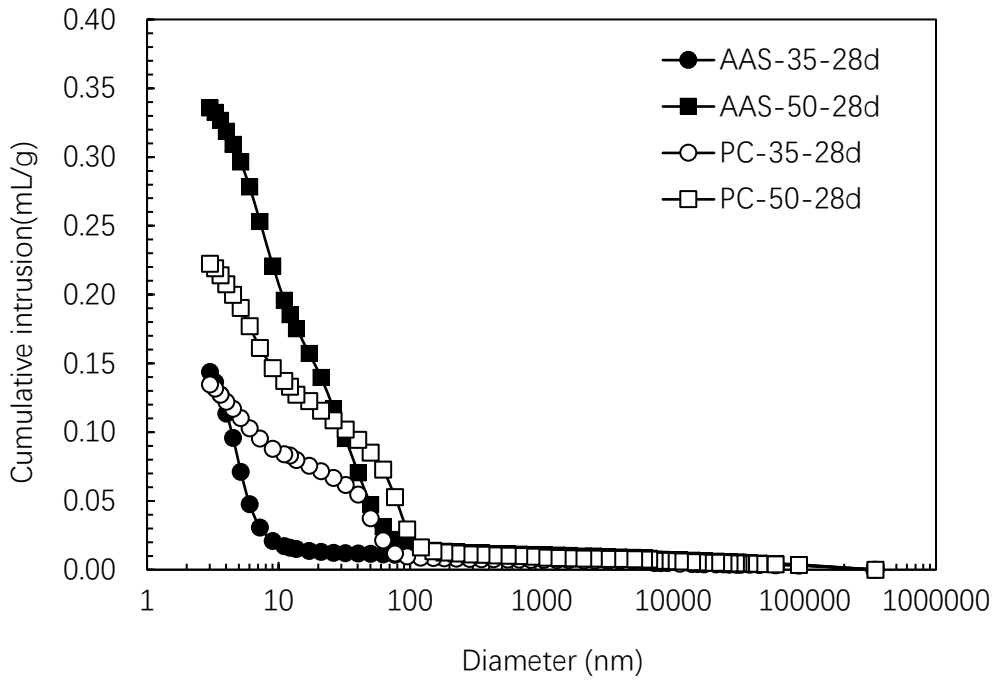
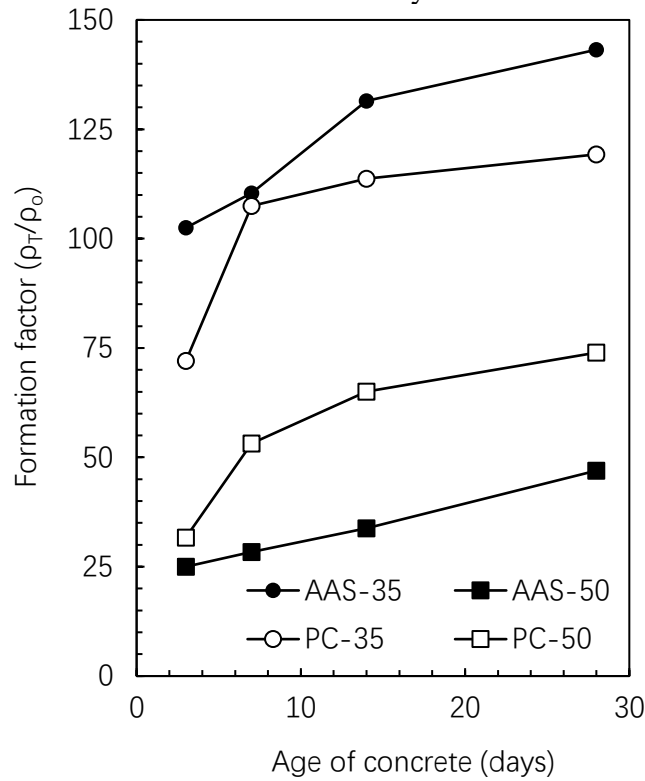


**Figure 5.** Pore size distribution of: (a) AAS pastes with W/B ratio 0.35 at 3, 7, 14 and 28 days; (b) PC pastes with W/B ratio 0.35 at 3, 7, 14 and 28 days; (c) comparison of pore volume ratio of AAS and PC pastes; (d) comparison of pore proportion based on the classification in (c).



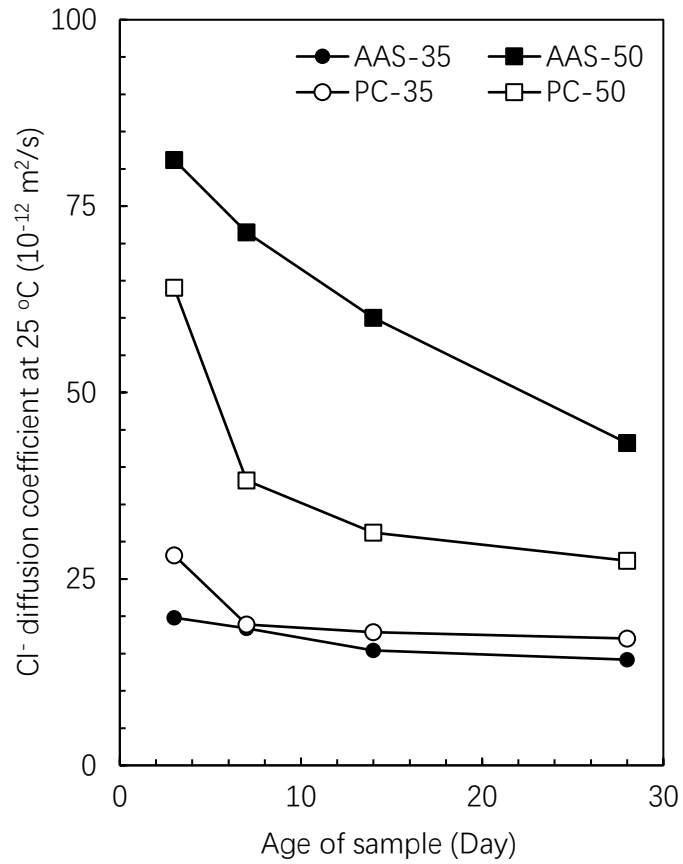
1  
2  
3

**Figure 6.** Comparison of the pore size distribution of AAS and PC pastes with 0.35 and 0.50 W/B ratios at 28 days

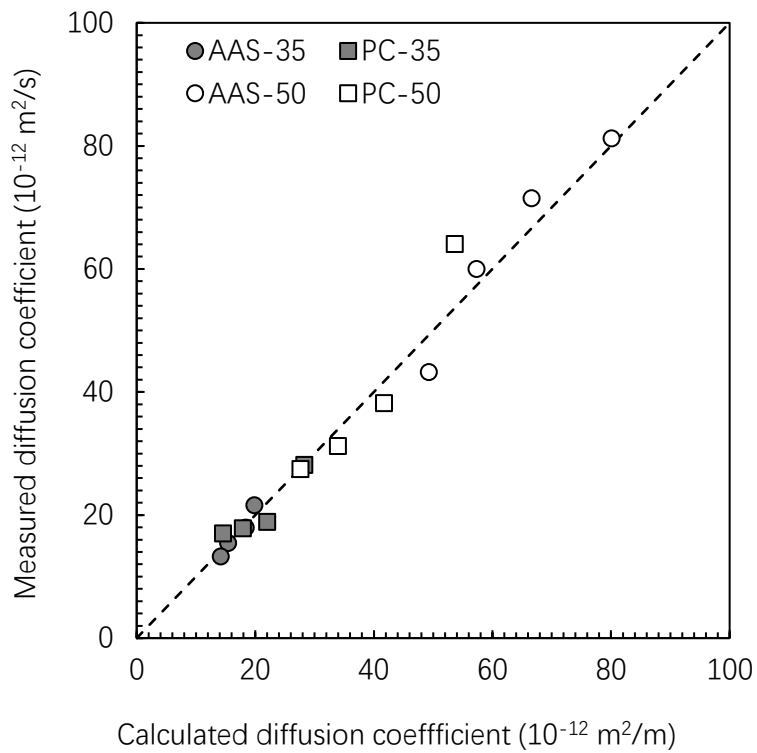


4  
5

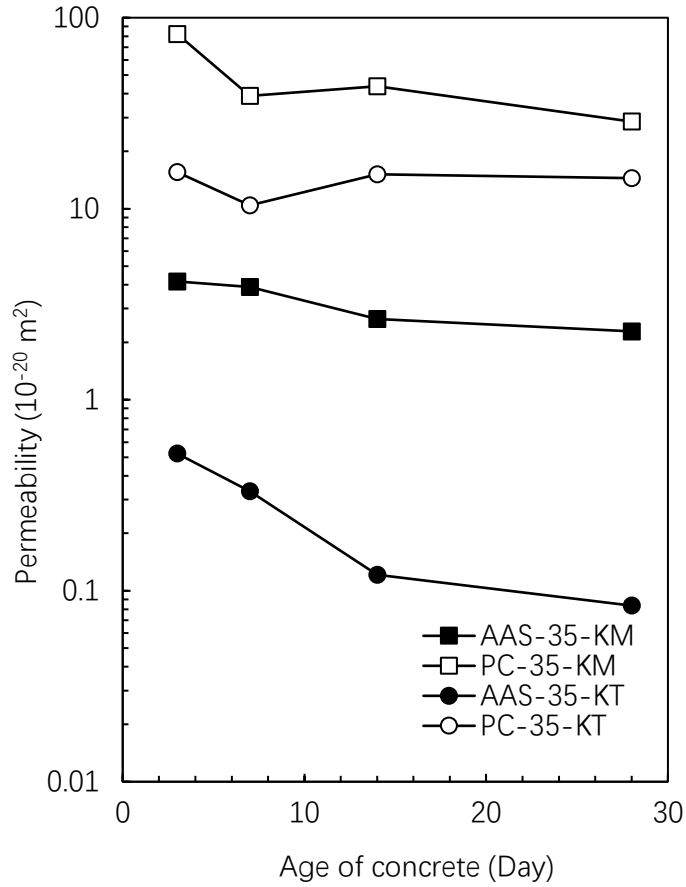
**Figure 7.** Temporal variation of formation factors for AAS and PC pastes



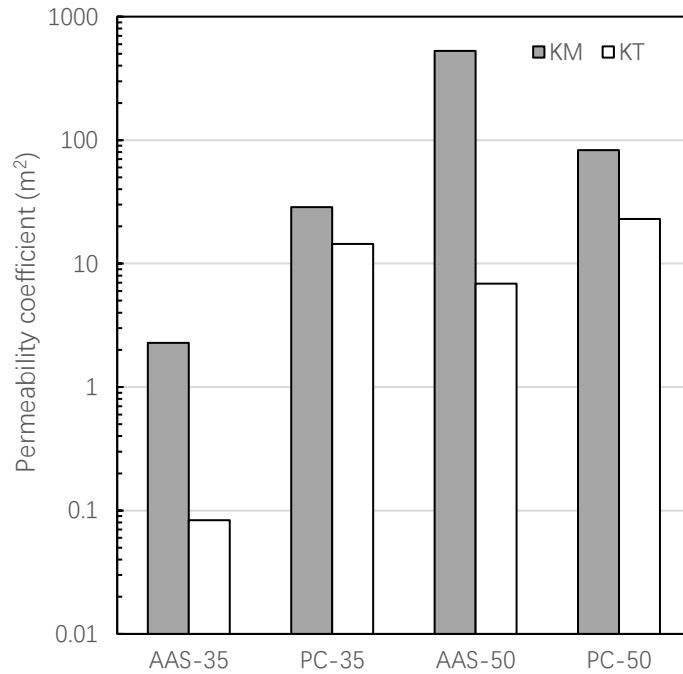
**Figure 8.** Temporal variation of Cl<sup>-</sup> diffusion coefficient for AAS and PC pastes



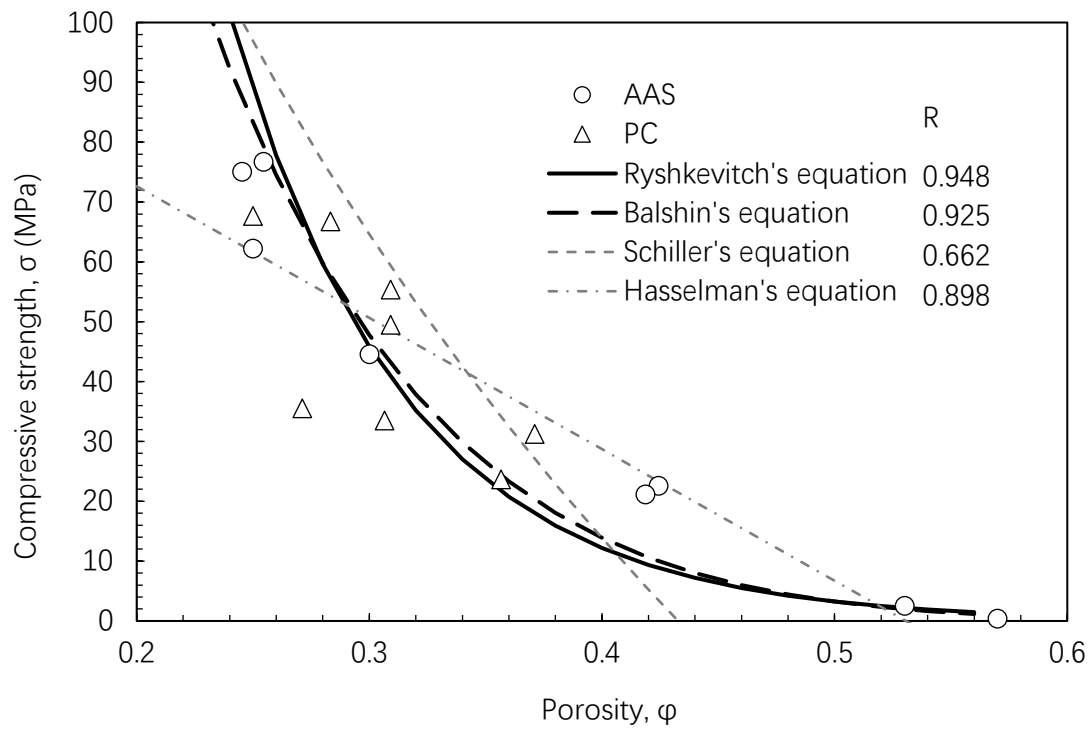
**Figure 9** Comparison between measured and estimated Cl<sup>-</sup> diffusion coefficients



**Figure 10** Comparison of estimated permeability coefficients for AAS and PC pastes



**Figure 11** Permeability coefficients of AAS and PC pastes with different W/B ratios estimated by MQ and KT models



1  
 2 **Figure 12.** Relationship between porosity and compressive strength of AAS and PC pastes  
 3  
 4